Available online at www.sciencedirect.com
ScienceDirect
Physics of the Earth and Planetary Interiors 160 (2007) 143–156
PHYSICS OF THE EARTH AND PLANETARY INTERIORS
www.elsevier.com/locate/pepi

Detecting thermal boundary control in surface flows from numerical dynamos

Julien Aubert [a,*], Hagay Amit [b], Gauthier Hulot [b]

[a] *Dynamique des Systèmes Géologiques, Institut de Physique du Globe de Paris, 4 place Jussieu, 75231 Paris Cedex 5, France*
[b] *Géomagnétisme, Institut de Physique du Globe de Paris, France*

Received 29 June 2006; received in revised form 30 October 2006; accepted 6 November 2006

Abstract

The geomagnetic field and secular variation exhibit asymmetrical spatial features which are possibly originating from an heterogeneous thermal control of the Earth's lower mantle on the core. The identification of this control in magnetic data is subject to several difficulties, some of which can be alleviated by the use of core surface flow models. Using numerical dynamos driven by heterogeneous boundary heat flux, we confirm that within the parameter space accessible to simulations, time average surface flows obey a simple thermal wind equilibrium between the Coriolis and buoyancy forces, the Lorentz, inertial and viscous forces playing only a secondary role, even for Elsasser numbers significantly larger than 1. Furthermore, we average the models over the duration of three vortex turnovers, and correlate them with a longer time average which fully reveals the signature of boundary heterogeneity. This allows us to quantify the possibility of observing mantle control in core surface flows averaged over a short time period. A scaling analysis is performed in order to apply the results to the Earth's core. We find that three vortex turnovers could represent between 100 and 360 years of Earth time, and that the heat flux heterogeneity at the core-mantle boundary could be large enough to yield an observable signature of thermal mantle control in a time average core surface flow within reach of the available geomagnetic data.

Keywords: Earth; Core; Dynamo; Geodynamo; Flows; Geomagnetism; Mantle; Thermal; Control; Coupling

1. Introduction

Over the last two decades many studies have been carried out to investigate possible intrinsically asymmetric spatial properties within the Earth's magnetic field. On the historical time scale, the secular variation (SV) of this field is quite heterogeneous (e.g. Bloxham and Gubbins, 1985; Jackson et al., 2000; Hulot et al., 2002), with a more active Atlantic hemisphere and a quieter Pacific hemisphere, and magnetic flux patches seemingly locked at remarkably stable spatial positions (Bloxham, 2002). It has also been suggested that the time average paleomagnetic (Gubbins and Kelly, 1993; Johnson and Constable, 1995) and archeomagnetic (Constable et al., 2000; Korte et al., 2005) fields show similar departures from axisymmetry as the modern historical field, although the robustness of such conclusions has been questioned by several authors (McElhinny et al., 1996; Carlut and Courtillot, 1998; Hongre et al., 1998) and is indeed difficult to assess without appropriate statistical tools (Hulot and Bouligand, 2005; Bouligand et al., 2005; Khokhlov et al., 2006).

The physical properties of the Earth's liquid core are however spatially homogeneous, and were the

* Corresponding author. Tel.: +33 144274796.
E-mail address: aubert@ipgp.jussieu.fr (J. Aubert).
URL: www.ipgp.jussieu.fr/~aubert (J. Aubert).

0031-9201/$ – see front matter © 2006 Elsevier B.V. All rights reserved.
doi:10.1016/j.pepi.2006.11.003

core-mantle boundary to impose homogeneous boundary conditions, no symmetry-breaking properties should arise in the time average behavior of the magnetic field created by the geodynamo, except possibly equatorial symmetry breaking properties which may arise spontaneously (Hulot and Bouligand, 2005; Bouligand et al., 2005). It is, therefore, generally thought that a longitudinal asymmetric signature within the geomagnetic field should reflect some spatially heterogeneous coupling at the CMB. Various coupling mechanisms have been proposed. Thermal control by the mantle, however, remains the most obvious and has indeed received much attention in the last decades (see for instance Hide, 1970; Jones, 1977; Bloxham and Gubbins, 1987). Given typical fluid velocities and heat diffusion constants at the base of the mantle, local temperature heterogeneities are likely to remain for millions of years, i.e. much longer than any time scale of core dynamics. Seen from the mantle, the rapidly mixed core is an isothermal boundary. Temperature anomalies in the mantle therefore translate into heat-flow anomalies (a colder mantle extracting more heat from the isothermal core). Since heat flow is continuous at the CMB, the core then "sees" the mantle as prescribing a steady and heterogeneous heat flow boundary condition.

Several difficulties hamper the identification of thermal mantle control in geomagnetic data. First, the signature of boundary heterogeneity is best seen when considering time averages (for instance Olson and Christensen, 2002; Bouligand et al., 2005) because transients usually mask the signal. Unfortunately, the needed averaging time is likely longer than the available geomagnetic time series. Autocorrelation functions of the geomagnetic field (Hulot and Le Mouël, 1994; Le Huy et al., 2000) indicate indeed that the signal loses memory of itself (a necessary condition for the removal of transients) on times of the order of several hundreds of years. A second difficulty is associated with the magnetic signature of thermal mantle control itself. Numerical dynamo models with heterogeneous heat flow at the outer boundary have shown that departures from the geocentric axial dipole are weak (Olson and Christensen, 2002) and difficult to distinguish from the statistical noise (Bouligand et al., 2005). The secular variation provides a clearer signature (Christensen and Olson, 2003) but it is difficult to formulate a simple theoretical link with the structure of boundary heterogeneity.

Core flows can be inverted at the core-mantle boundary (CMB) of the Earth from the historical magnetic field and SV observations (recently Hulot et al., 2002; Amit and Olson, 2004). Summarizing all the available information into a fluid dynamical framework, they tend to suffer less from the difficulties mentioned above. Their autocorrelation time is shorter (Le Huy et al., 2000), because the advection of momentum is much more turbulent than the advection of the magnetic field, as a result of the large ratio of magnetic diffusivity to viscosity in the Earth's core. Furthermore, a simple thermal wind theory is expected to connect them with CMB heat flow hetereogeneities (Bloxham and Gubbins, 1987; Bloxham and Jackson, 1990), although questions remain concerning the role of the Lorentz force, which will be addressed in the present study. Finally, they preserve the spatial asymmetry of the original data (Amit and Olson, 2006): the Atlantic/Pacific dichotomy, as well as stable vortices (specifically in the southern hemisphere). In addition heterogeneity is also present between the northern and southern hemispheres, with significant westward drift at mid-latitude of the southern hemisphere but nearly no drift at mid-latitude of the northern hemisphere (Pais and Hulot, 2000; Amit and Olson, 2006). In this line of work, several studies compared core flows models with the time average outcome of numerical convection models driven by heterogeneous thermal boundary conditions, especially focusing on the interaction of convection structures with the boundary heat flow pattern (Zhang and Gubbins, 1992, 1993; Gibbons and Gubbins, 2000).

Previous studies have shown that core flows also need time-averaging to reveal the mantle signature. A central question remains: how long should the time-average be in order to remove enough of the transients? We anticipate that this should be shorter than for the magnetic field, and the first goal of the present study is precisely to assess this. Amit and Olson (2006) used the historical geomagnetic SV data to infer a time-average flow model for the period 1840–1990. Is such an averaging interval enough to reveal the core flow driven by boundary heterogeneity? To address this question we focus on self-consistent numerical models of convective dynamo action with heterogeneous boundary heat flow, and produce two types of flows: snapshots, and averages over intermediate intervals which we argue would cover 100–360 years of real Earth time once properly rescaled. These flows are compared to the actual steady flow computed by averaging over the entire simulation time. A statistical analysis of the correlation coefficient between the intermediate flows and the steady flow then provides us with a quantitative way to assess the likeliness of revealing mantle control in time-average core surface flows. This study also provides an opportunity to investigate core surface fluid flows, in very much the same way as Olson and Christensen (2002) investigated the magnetic field. Finally it makes it possible to discuss more quantitatively the possibility that certain robust fea-

tures of SV inversion core flows could indeed be due to thermal control from the mantle.

2. Numerical model

2.1. Formulation

We model thermal convection and self-sustained dynamo action in a rotating spherical shell. A spherical coordinate system (r, θ, φ) with unit vectors $(\mathbf{e}_r, \mathbf{e}_\theta, \mathbf{e}_\varphi)$ is chosen. The magnetohydrodynamic equations for the velocity $\mathbf{u}$, magnetic induction $\mathbf{B}$, temperature T and pressure P are solved for a conducting and convecting Boussinesq fluid within a spherical shell between radii r_i and r_o, the aspect ratio r_i/r_o being fixed to 0.35 as for the liquid outer core of the Earth. The shell is rotating about the $\mathbf{e}_z$ axis of rotation. We adopt the dimensionless form chosen by Christensen and Aubert (2006), with a slight modification to account for a fixed heat flux boundary condition at the outer boundary:

$$\frac{\partial \mathbf{u}}{\partial t} + \mathbf{u}\cdot\nabla\mathbf{u} + 2\mathbf{e}_z \times \mathbf{u} + \nabla P = Ra_\kappa \frac{\mathbf{r}}{r_o} T + (\nabla + \mathbf{B}) \times \mathbf{B} + E\nabla^2\mathbf{u} \quad (1)$$

$$\frac{\partial \mathbf{B}}{\partial t} = \nabla \times (\mathbf{u} \times \mathbf{B}) + E_\lambda \nabla^2 \mathbf{B} \quad (2)$$

$$\frac{\partial T}{\partial t} + \mathbf{u}\cdot\nabla T = E_\kappa \nabla^2 T \quad (3)$$

$$\nabla \cdot \mathbf{u} = 0 \quad (4)$$

$$\nabla \cdot \mathbf{B} = 0 \quad (5)$$

The inverse of the rotation rate Ω^{-1} is chosen as time scale. The length scale is the shell thickness D. The magnetic induction is scaled by $(\rho\mu)^{1/2}\Omega D$, where ρ is the fluid density and μ the magnetic permeability of the fluid. The temperature is scaled by

$$\Delta T = \frac{q_0 D}{\rho C_p \kappa} \quad (6)$$

where q_0 is the homogeneous part of the heat flux per unit surface, C_p the specific heat of the fluid and κ is the thermal diffusivity. The dimensionless parameters are the Rayleigh number Ra_κ and the thermal, magnetic and viscous Ekman numbers E_κ, E_λ and E:

$$Ra_\kappa = \frac{\alpha g_o q_0}{\rho C_p \Omega^2 \kappa} \quad (7)$$

$$E_\kappa = \frac{\kappa}{\Omega D^2} \quad (8)$$

$$E_\lambda = \frac{\lambda}{\Omega D^2} \quad (9)$$

$$E_\lambda = \frac{\nu}{\Omega D^2} \quad (10)$$

Here α is the thermal expansion coefficient, g_o the gravity at the outer boundary, λ is the magnetic diffusivity and ν is the viscosity of the fluid. The reader may be more familiar with the Prandtl and magnetic Prandtl numbers $Pr = \nu/\kappa$ and $Pm = \nu/\lambda$ which will be reported in our Table 1 of numerical simulations.

The velocity field satisfies rigid boundary conditions. The magnetic field satisfies insulating boundary conditions. Although treating the inner core as an insulator is non-physical, the influence of inner-core conductivity is indeed thought to be insignificant (Wicht, 2002). The inner boundary has a constant and uniform temperature. A spatially heterogeneous heat flow is prescribed at the outer boundary, the influence of which we wish to investigate. Following Olson and Christensen (2002) the level of this heterogeneity is quantified by the parameter

$$q^* = \frac{q_{max} - q_{min}}{2q_0} \quad (11)$$

representing half the ratio of the peak-to-peak amplitude of the heterogeneity to the average heat flux q_0.

The numerical implementation MAGIC by Johannes Wicht is used in this study (Wicht, 2002).

2.2. Numerical data set, methods and outputs

Table 1 summarizes the different numerical calculations which have been performed. Cases q00 and q06 are reproductions of cases already published in Olson and Christensen (2002). Case T1 is similar to the "tomographic" dynamo of these authors. Our choice of values for q^* is subject to several constraints. Obviously q^* is bound to zero on the low side (no mantle control), whereas, dynamo action is lost for too large values of q^* (Olson and Christensen, 2002). We show in Section 3.1 that the product $q^* Ra_\kappa$ is the main scaling parameter for the amplitude of steady, boundary-driven flow. In Section 4, we estimate the values of q^* and Ra_κ in the Earth's core and show that numerical simulations can reach Earth-like values of $q^* Ra_\kappa$. We, therefore, use lower values of Ra_κ, and higher values of q^* than in the Earth's core, while maintaining Earth-like values of $q^* Ra_\kappa$.

In most calculations the heat flow heterogeneity has been reduced to a single spherical harmonic (denoted by Y_l^m as in Olson and Christensen (2002)) to facilitate the understanding of the results. For the real Earth a more complex boundary condition should obviously be used. The heat flow heterogeneity at the CMB is poorly known, and usually assumed to be correlated with seismic shear velocity at the base of the mantle (e.g. Olson

Table 1
Set of numerical models (see text for details)

Case	Pattern	q^*	Ra_κ	E_κ	Pm	Pr	U	U_{ave}	Pe	δ	Λ	τ_{ave}/τ_u
q00	None	0	0.225	3×10^{-4}	2	1	2.14×10^{-2}	0	71.3	–	5.4	497
q01	Y_2^2	0.1	0.225	3×10^{-4}	2	1	2.15×10^{-2}	1.80×10^{-3}	71.7	0.130	5.3	213
q02	Y_2^2	0.2	0.225	3×10^{-4}	2	1	2.15×10^{-2}	2.20×10^{-3}	71.7	0.079	5.2	215
q04	Y_2^2	0.4	0.225	3×10^{-4}	2	1	2.21×10^{-2}	3.89×10^{-3}	73.7	0.069	4.7	515
q04h	Y_2^2	0.4	0.45	3×10^{-4}	2	1	3.33×10^{-2}	1.15×10^{-2}	111.2	0.088	4.5	280
q06	Y_2^2	0.625	0.225	3×10^{-4}	2	1	2.21×10^{-2}	5.56×10^{-3}	73.7	0.061	4.7	589
Pr03	Y_2^2	0.625	0.75	10^{-3}	2	0.3	7.85×10^{-2}	2.90×10^{-2}	78.5	0.087	14.9	80
hh	Y_2^2	0.625	0.675	3×10^{-4}	2	1	4.18×10^{-2}	1.68×10^{-2}	139.3	0.056	5.4	238
ll	Y_2^2	0.625	0.0315	3×10^{-5}	2	1	3.00×10^{-3}	4.59×10^{-4}	100	0.062	12.2	50
lh	Y_2^2	0.625	0.18	3×10^{-5}	1	1	8.57×10^{-3}	2.52×10^{-3}	285.7	0.032	8.1	89
q08	Y_2^2	0.8	0.225	3×10^{-4}	2	1	2.30×10^{-2}	7.83×10^{-3}	76.7	0.060	3.6	307
Y21-2	Y_2^1	0.2	0.225	3×10^{-4}	2	1	2.17×10^{-2}	1.97×10^{-3}	72.2	0.141	5.1	364
Y21-1	Y_2^1	0.625	0.225	3×10^{-4}	2	1	2.17×10^{-2}	4.31×10^{-3}	72.3	0.129	5.4	290
Y21-3	Y_2^1	0.39	0.36	3×10^{-4}	2	1	2.88×10^{-2}	5.52×10^{-3}	96.1	0.120	4.8	404
Y21-4	Y_2^1	0.625	0.36	3×10^{-4}	2	1	2.90×10^{-2}	8.18×10^{-3}	96.7	0.112	4.8	119
Y21-5	Y_2^1	0.625	0.675	3×10^{-4}	2	1	4.75×10^{-2}	1.22×10^{-3}	158	0.085	0.9	130
T2	Tomo	0.2	0.225	3×10^{-4}	2	1	2.14×10^{-2}	1.13×10^{-3}	71.3	0.091	5.4	369
T1	Tomo	0.5	0.225	3×10^{-4}	2	1	2.14×10^{-2}	2.49×10^{-3}	71.3	0.097	5.7	357
T3	Tomo	0.31	0.36	3×10^{-4}	2	1	2.85×10^{-2}	5.07×10^{-2}	95.2	0.107	4.8	144
T4	Tomo	0.4	0.36	3×10^{-4}	2	1	2.88×10^{-2}	4.70×10^{-3}	96	0.065	4.7	251
T5	Tomo	0.93	0.36	3×10^{-4}	2	1	2.98×10^{-2}	7.5×10^{-3}	99.3	0.051	3.5	287
T6	Tomo	0.5	0.675	3×10^{-4}	2	1	4.44×10^{-2}	1.1×10^{-2}	148.1	0.071	2.4	138
S1	Y_2^2	0.625	2.25×10^{-4}	3×10^{-4}	2	1	3×10^{-5}	4.31×10^{-5}	0.1	0.693	0	Steady flow
S2	Tomo	0.5	2.25×10^{-4}	3×10^{-4}	2	1	1.414×10^{-5}	1.80×10^{-5}	0.047	0.57	0	Steady flow

and Christensen, 2002): regions of the mantle with high seismic shear velocity are supposedly colder than average, extracting more heat from the core. Note that this assumption allows to prescribe the pattern, but not the amplitude, of boundary heterogeneities. Note also that explaining seismic shear velocity variations in terms of temperature alone is quite a crude assumption because it entirely ignores possible contributions from chemical heterogeneities as well as possible phase transitions above the CMB. Obviously, it would be desirable to separate thermal and chemical contributions to the seismic anomalies. Such a decomposition has in fact been tentatively introduced by Trampert et al. (2004), but only with a sub-family of spherical harmonic components. Despite the lack of information, a multi-harmonic boundary condition should be included in order to render geophysically relevant non-linear effects. In cases T1–T6 and S2 (hereafter also labelled as tomographic cases) we have used the pattern of the seismic shear velocity model of Masters et al. (2000) at the base of the mantle. This pattern contains little energy after spherical harmonic degree 8 and is therefore truncated at this degree.

In cases S1 and S2 (hereafter also labelled as subcritical cases) the Rayleigh number has been set to a value below the critical value for convection onset. The fluid is then stably stratified and the system responds only to the lateral heat flow heterogeneity imposed at the outer boundary. Obviously cases S1 and S2 are not dynamos. All other cases but case Y21-5 produce a self-sustained magnetic field with a non-reversing axial dipole. Case Y21-5 presents a weaker axial dipole with excursions. The time-average magnetic field and secular variation produced by heterogeneous dynamos has been studied in detail by Olson and Christensen (2002), Christensen and Olson (2003) and is not within the general scope of the present study. However, for a crude estimate of the relative importance of the Lorentz force in the system, we have reported in Table 1 the value of the Elsasser number defined as:

$$\Lambda = \frac{1}{E_\lambda V}\left\langle \int_V \mathbf{B}^2 \, \mathrm{d}V \right\rangle_{\tau_{\mathrm{ave}}} \tag{12}$$

Angular brackets denote time-averaging. The averaging time τ_{ave} is the duration of the run. The shell volume is denoted by V.

In this study, the root-mean-squared, time average velocity in the shell is defined as

$$U = \sqrt{\left\langle \frac{1}{V}\int_V \mathbf{u}^2 \, \mathrm{d}V \right\rangle_{\tau_{\mathrm{ave}}}} \tag{13}$$

Due to the choice of $1/\Omega$ as time scale, U is a Rossby number of the flow. To quantify the importance of thermal advection versus diffusion of heat, we introduce the classical Péclet number

$$Pe = \frac{\tilde{U} D}{\kappa} \tag{14}$$

where we generally denote with a tilde the value of variables in the dimensional world (for the present instance $\tilde{U} = U\Omega D$). In the non-dimensional world, we have therefore

$$Pe = \frac{U}{E_\kappa} \tag{15}$$

Also derived from $\tilde{U}$ is the advection time, or vortex turnover time $\tilde{\tau}_u$:

$$\tilde{\tau}_u = \frac{D}{\tilde{U}} \tag{16}$$

In the non-dimensional world, we simply have

$$\tau_u = \frac{1}{U} \tag{17}$$

Numerical models are run until energetic equilibration. The steady flow is then extracted by a further calculation averaged over a time τ_{ave} ranging from 50 (for the most demanding calculations), to 500 vortex turnover times. The vortex turnover time is the fundamental time scale for mixing, and the steady flow therefore corresponds to a well-mixed thermal state where the effect of heterogeneous heat flow boundary conditions appears.

On a shorter time interval made of fewer vortex turnovers, average flows are associated with an incomplete thermal mixing. We now attempt to estimate the vortex turnover time in the Earth's core, in a manner consistent with (13) and (16). A conventional range of values for the velocity close to the CMB is 3×10^{-4} m/s to 5×10^{-4} m/s (Bloxham and Jackson, 1991; Eymin and Hulot, 2005). According to the numerical dynamos of Christensen and Aubert (2006), surface flow magnitudes have to be amplified by a factor 2–4 to get root-mean-squared flow velocities inside the core, yielding estimates of $U = 6 \times 10^{-4}$ to 2×10^{-3} m/s. The estimate for the vortex turnover hence ranges from 35 to 120 years. This range is consistent with the typical auto-correlation times computed from core surface flows inferred from the historical geomagnetic data (Le Huy et al., 2000). To determine the likeliness that core flows time averaged over historical time periods contain a signature of mantle control, we, therefore, define intermediate flows averaged over $3\tau_u$ time units of the simulation, and compare them to fully converged time-averages. For the real Earth, considering a duration of

three vortex turnovers corresponds to performing time averages over historical periods of 100–360 years. It must be stressed that our approach is equivalent to matching the non-dimensional time in numerical simulations to the actual time in the Earth's core through the advection, or vortex turnover time. We are well aware that this choice is quite uncommon, because the Reynolds number in numerical dynamos (which represents the amount of momentum advection with respect to viscous diffusion) has a typical value of a few hundreds and is very remote from Earth's core values of order 10^8 (Christensen and Aubert, 2006). The magnetic Reynolds number (which is the equivalent of the Reynolds number for magnetic advection) is more Earth-like in numerical dynamos, and this often motivates the choice to re-scale non-dimensional time to Earth's core time through the magnetic dipole decay time (see for instance Christensen and Tilgner (2004)). This is, however, of little use in the present study since we focus on flow and thermal features rather than on magnetic field features. We rather attempt to capture the mixing effect of three large-scale vortex turnovers, while the effect of smaller-scale, unresolved vortices is represented by an overestimated viscosity.

Flows will be examined on a spherical surface S located below the core-mantle boundary, at the top of the free stream, outside the viscous Ekman layer. The homogeneous dynamo drives a significant part of the zonal flow observed on S (Aubert, 2005). This part must be removed in order to avoid spurious positive correlations that are unrelated with our ability to retrieve mantle control. Since it is technically difficult to isolate the homogeneous dynamo zonal flow at all time scales, we simply use the non-axisymmetric velocity field $\mathbf{u}_{\rm na}$ and temperature field $T_{\rm na}$. The amplitude $U_{\rm ave}$ of the boundary-induced, steady flow is defined as:

$$U_{\rm ave} = \sqrt{\frac{1}{S}\int_S \langle \mathbf{u}_{\rm na}\rangle^2_{\tau_{\rm ave}}\ {\rm d}S} \tag{18}$$

We also define a thermal penetration depth δ as

$$\delta = \left(\frac{1}{S}\int_S \langle T_{\rm na}\rangle^2_{\tau_{\rm ave}}\ {\rm d}S\right)^{1/2}\left(\frac{1}{S}\int_S \left\langle \frac{\partial T_{\rm na}}{\partial r}\right\rangle^2_{\tau_{\rm ave}}\ {\rm d}S\right)^{-1/2} \tag{19}$$

The intermediate and steady flows will be compared through a standard vector correlation coefficient

$$C_{\rm int} = \frac{\int_S \langle \mathbf{u}_{\rm na}\rangle_{3\tau_u}\cdot\langle \mathbf{u}_{\rm na}\rangle_{\tau_{\rm ave}}\ {\rm d}S}{\sqrt{\int_S \langle \mathbf{u}_{\rm na}\rangle^2_{3\tau_u}\ {\rm d}S}\sqrt{\int_S \langle \mathbf{u}_{\rm na}\rangle^2_{\tau_{\rm ave}}\ {\rm d}S}} \tag{20}$$

Instantaneous correlation coefficients will also be computed using flow snapshots:

$$C = \frac{\int_S \mathbf{u}_{\rm na}\cdot\langle \mathbf{u}_{\rm na}\rangle_{\tau_{\rm ave}}\ {\rm d}S}{\sqrt{\int_S \mathbf{u}^2_{\rm na}\ {\rm d}S}\sqrt{\int_S \langle \mathbf{u}_{\rm na}\rangle^2_{\tau_{\rm ave}}\ {\rm d}S}} \tag{21}$$

Obviously, C and $C_{\rm int}$ are variable in time because snapshots and incomplete time averages are time-dependent. A statistical approach is therefore adopted. For each numerical model, 10 independent realizations of C and $C_{\rm int}$ are performed, in order to extract the mean and standard deviation of the correlation coefficients.

3. Results

3.1. The steady flow

In this study, the steady flow serves as a reference for detecting the signature of mantle control. In early studies of heterogeneous mantle control (Zhang and Gubbins, 1992, and followers) it was shown that a thermal wind balance between the buoyancy and Coriolis vorticities drives the flow at the top of the free stream. However, these studies used models of non-magnetic convection, which are unlikely to be relevant to the real core since the flow may change much in the presence of a magnetic field (Olson and Glatzmaier, 1996). The exact influence of the Lorentz force at the top of the core is not well-known. The hypothesis that it is weak is grounding the tangential geostrophy assumption (Le Mouël et al., 1985) that is commonly used in core flow inversion from geomagnetic SV data (Hulot et al., 2002). Here, we first clarify the role of the Lorentz force in the numerical models.

As in Christensen and Aubert (2006) we write the curled version of Eq. (1) to obtain an equation for the vorticity $\omega = \nabla\times\mathbf{u}$:

$$\frac{\partial\omega}{\partial t} + \nabla\times(\omega\times\mathbf{u}) - 2\frac{\partial\mathbf{u}}{\partial z} = \frac{Ra_\kappa}{r_{\rm o}}\nabla\times(T\mathbf{r}) + \nabla\times[(\nabla\times\mathbf{B})\times\mathbf{B}] + E\nabla^2\omega \tag{22}$$

The thermal wind balance holds when the Coriolis vorticity $-2\partial\mathbf{u}/\partial z$ is balanced by the buoyancy vorticity $Ra_\kappa/r_{\rm o}\nabla\times(T\mathbf{r})$. The two horizontal components of this balance are checked at the top of the free stream, for the steady flow, in Fig. 1. The azimuthal component shows a well-respected balance, dominated by the axisymmetric component. This is in agreement with the findings of Aubert (2005): the steady zonal flow in homogeneous dynamos is mainly a thermal wind. The meridional component reveals more the quality of the balance for non-axisymmetric flows driven by the heterogeneous boundary condition. The agreement, while being less

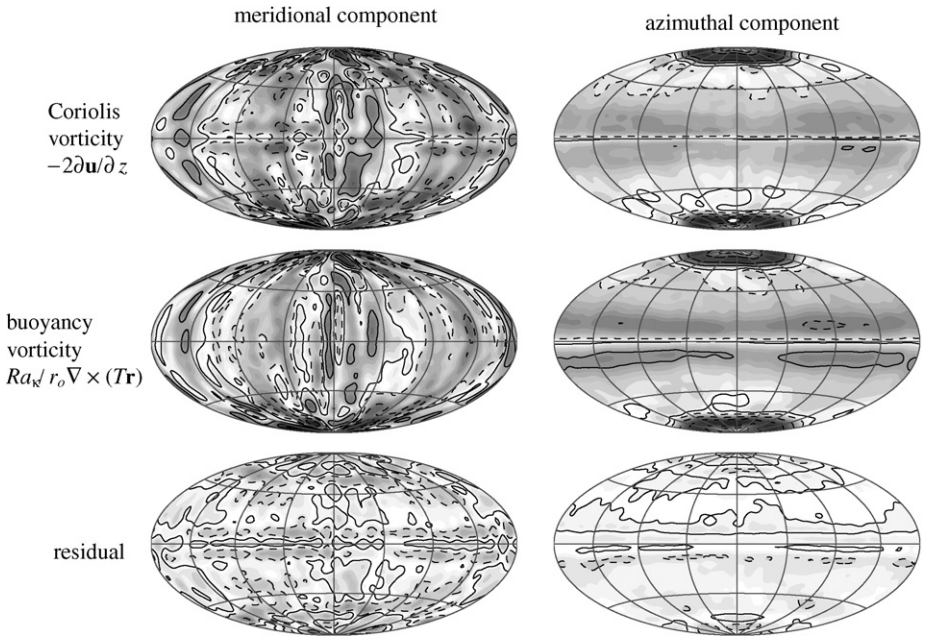

Fig. 1. Long-term (τ_{ave}) time average of case q04. Check of the meridional (contour interval 0.09, plain contours are positive values, dashed contours are negative values) and azimuthal (contour interval 0.03) thermal wind balance at depth 0.07. The residual represents the deviation of the vorticity balance from thermal wind. The root-mean-squared residual amplitude represents 33% (meridional) and 20% (azimuthal) of the root-mean-squared curled force amplitude.

satisfactory (especially near the equator where thermal wind is expected to fail) still shows a good degree of correlation with a low residual. The Lorentz force makes for most of this residual, while inertia and viscosity play a secondary role in this case (not shown here). At first glance it may seem surprising that the Lorentz force does not perturb the system from a thermal wind balance. However, one must bear in mind that the magnetic pressure, which represents a sizeable part of this force, does not enter the curled force balance (22), reducing the contribution of the Lorentz force, even when the Elsasser number Λ is clearly above 1 (for case q04 we have $\Lambda = 4.7$).

Now that we are confident that steady flows of the heterogeneous dynamos can reasonably be described in terms of thermal winds, we may propose a scaling for their amplitude, which will be useful to quantify their importance versus transient flows. The thermal wind balance writes

$$-2\frac{\partial \mathbf{u}}{\partial z} = \frac{Ra_\kappa}{r_o} \nabla \times (T\mathbf{r}) \tag{23}$$

The $\nabla\times$ operator acting on $T\mathbf{r}$ introduces a length scale in the lateral direction. The z-derivative on the left-hand-side contains radial and lateral length scales. In a thick spherical shell, both can be anticipated to be of the same order of magnitude. The left-hand side and right-hand side length scales therefore cancel in the scaling for U_{ave} which writes:

$$2U_{ave} \approx Ra_\kappa T_{ave} \tag{24}$$

Here T_{ave} is the typical amplitude of the temperature variations associated with the thermal wind U_{ave}. In the non-dimensional form introduced by (6), the Fourier law of heat conduction writes:

$$q = -\frac{\partial T}{\partial r} \tag{25}$$

Hence, a scaling for T_{ave} is obtained by using the thermal penetration depth δ and the amplitude of heat flux heterogeneity q^*:

$$T_{ave} \approx 2q^*\delta \tag{26}$$

Note that the factor 2 here is due to the fact that T_{ave} represents a peak-to-peak variation, while q^* is a zero-to-peak value. The scaling for U_{ave} writes

$$\frac{U_{ave}}{\delta} \approx q^* Ra_\kappa \tag{27}$$

The proposed scaling is checked in Fig. 2. For the Y_2^2 pattern (circles, diamonds and cross), U_{ave}/δ linearly grows with q^* and with Ra_κ, with a slope of 0.72, close to the theoretical slope 1. Moreover, a given value of the product $q^* Ra_\kappa$ yields a unique thermal wind amplitude. This response is checked against various values of Ra_κ, E_κ

and Pr. For Y_2^1 and tomographic patterns the linearity still mostly holds, with lower slopes of 0.45 (tomographic) and 0.33 (Y_2^1). Indeed these patterns contain equator-antisymmetric forcing components, which oppose the Proudman-Taylor constraint of the rotating system to set up a flow.

The Y_2^1 and tomographic patterns have, however, an additional peculiarity when compared to Y_2^2: looking for instance at cases T1 and T3 (or Y21-1 and Y21-3, T5 and T6) we see that it is possible to obtain slightly different thermal wind values (within a factor 2) for two sets of (q^*, Ra_κ), while maintaining a constant value for the product $q^* Ra_\kappa$. Due to the Proudman-Taylor constraint, equator-symmetric and antisymmetric patterns induce different responses. In the Y_2^2 cases the homogeneous (Ra_κ) and heterogeneous (q^*) forcings are both equator-symmetric, so the roles of q^* and Ra_κ can be swapped (for instance cases q04h and q08 yield almost exactly the same $U_{\rm ave}/\delta$). In the Y_2^1 and tomographic cases, the heterogeneous forcing is no longer equator-symmetric, and this breaks the symmetry between q^* and Ra_κ. Different behaviors of equator-symmetric and antisymmetric forcings were already observed by Gibbons and Gubbins (2000). While the symmetry-breaking between q^* and Ra_κ can influence the thermal wind amplitude, it certainly does not change its order of magnitude. We conclude that the response is still mostly linear.

Fig. 2 shows that, for a given flow pattern and as predicted by (27), the amplitude of the steady flow responds mostly linearly to the level of imposed mantle heterogeneity $q^* Ra_\kappa$ if we correct for the thermal penetration depth δ. The nonlinear part of the response is hidden in δ, which is crucially sensitive to advection and mixing of heat. To provide a scaling for δ, we first assimilate δ to a thermal boundary layer thickness (although the limitations of this hypothesis will be shown below). In a classical Rayleigh-Benard system without rotation, the dimensional $\tilde{\delta}$ correlates then with the thermal diffusion length $\sqrt{\kappa D/\tilde{U}}$. Due to the presence of a dominant Coriolis force, it is expected that core flows behave differently. It is possible to derive a scaling for the thermal boundary layer thickness in rotating dynamos from the extensive parameter space study of Christensen and Aubert (2006), starting from their scaling $Nu^* \propto (Ra_Q^*)^{0.5}$ tying their modified Nusselt Nu^* and Rayleigh Ra_Q^* numbers

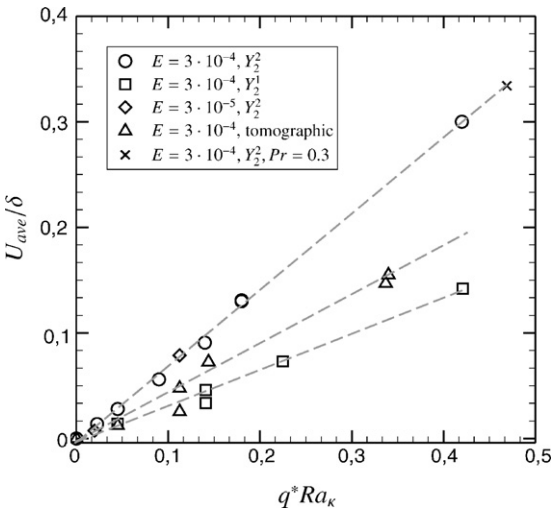

Fig. 2. Amplitude $U_{\rm ave}$ of the steady thermal wind, corrected for the thermal penetration depth δ as a function of the scaling parameter $q^* Ra_\kappa$. The three dashed lines represent the respective fits $U_{\rm ave}/\delta = 0.72,\ 0.45,\ 0.33\ q^* Ra_\kappa$ for cases with Y_2^2, tomographic and Y_1^2 heat flow patterns.

$$Nu^* = \frac{r_o}{r_i}\frac{q_{\rm adv}}{\rho C_p \Delta T \Omega D} \tag{28}$$

$$Ra_Q^* = \frac{r_o}{r_i}\frac{\alpha g_0 q_{\rm adv}}{\rho C_p \Omega^3 D^2} \tag{29}$$

Only the advective part $q_{\rm adv}$ of the total heat flux q_0 escaping from the core enters the formulas above. In their models the temperature difference ΔT is prescribed between the inner and the outer sphere of the shell. We have a different choice of boundary conditions, where ΔT is a variable while q_0 is prescribed. To adapt their result, we use Fourier's law to relate ΔT with q_0 using the thermal penetration depth $\tilde{\delta}$:

$$q_0 = \rho C_{\rm p} \kappa \frac{\Delta T}{2\tilde{\delta}} \tag{30}$$

Considering only sufficiently forced models so that $q_0 \approx q_{\rm adv}$ an expression for Nu^* as a function of δ follows:

$$Nu^* \approx \frac{r_o}{r_i}\frac{E_\kappa}{\delta} \tag{31}$$

and we also have

$$Ra_Q^* = \frac{r_o}{r_i} Ra_\kappa E_\kappa \tag{32}$$

so that the Christensen and Aubert (2006) scaling finally relates δ with control parameters:

$$\delta \propto \left(\frac{Ra_\kappa}{E_\kappa}\right)^{-0.5}. \tag{33}$$

In Fig. 3, a power-law fit for supercritical cases with Y_2^2 heat flow pattern yields $\delta = 1.1(Ra_\kappa/E_\kappa)^{-0.4}$, in reasonable agreement with (33). Assimilating δ to a thermal boundary layer thickness obviously fails to describe its sensitivity to q^* (circles aligned along a vertical). However q^* is bound by the need to maintain a dynamo (Olson

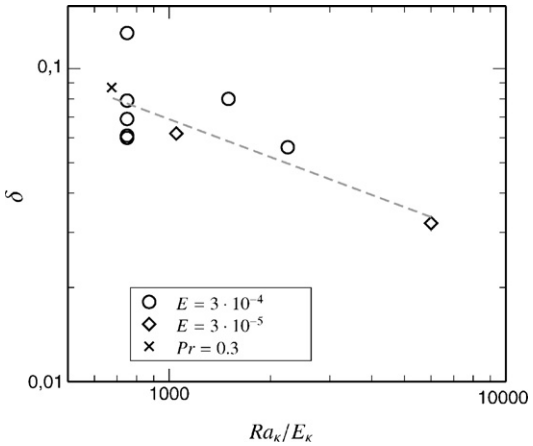

Fig. 3. Y_2^2 heat flow pattern. Scaling of the thermal penetration depth δ according to Christensen and Aubert (2006). The best-fit power law is $\delta = 1.1(Ra_\kappa/E_\kappa)^{-0.4}$.

and Christensen, 2002) and can certainly not influence δ on a range larger than that indicated on Fig. 3.

The advection of temperature alters the magnitude, but also the structure of the steady flow, especially when the boundary heterogeneity pattern has a complex spectral content such as in the tomographic cases T1 and S2. Fig. 4a shows the heat flow pattern used in these cases. In Fig. 4b we first show the pattern of sub-critical response (case S2) to this heat flow, with no underlying convection. The temperature field is simply a smoothed (due to thermal diffusion) image of the prescribed heat flow, and the resulting thermal wind is rather equatorially symmetric. Fig. 4c presents the supercritical response (case T1). For the purpose of comparison with Fig. 4b, the steady contribution from the homogeneous dynamo case q00 (which has the same parameters as case T1 except the value of q^*), which is entirely zonal, has been removed. The flow pattern is similar to that obtained by Olson and Christensen (2002, Fig. 9b), and Gibbons and Gubbins (2000, Fig. 4c). Here the temperature structure results from two effects: the imposed boundary heterogeneity as in Fig. 4b, but also the underlying thermal mixing, which drastically reduces the depth δ of penetration of the boundary condition, from one half of the shell in Fig. 4b to one tenth of the shell in Fig. 4c (see Table 1). The flow pattern driven by the mixed temperature heterogeneity is now quite asymmetric, with only two strong vortices (southern Atlantic and northern American) and quieter zones such as the southern Pacific.

Another interesting effect of temperature advection is the longitudinal angular shift between the imposed heat flow pattern and the flow vortices. Indeed a comparison between Fig. 4b and c reveals that the main African temperature patch and its associated vortex are

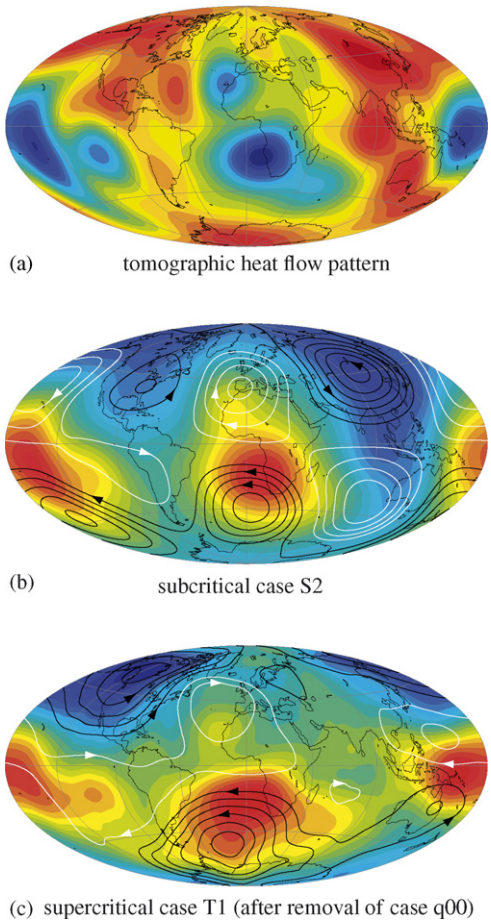

Fig. 4. (a) Heat flow pattern used in cases S2 and T1, derived from the Masters et al. (2000) seismic shear velocity model (larger than average outwards heat flux in red). (b and c) streamfunction representations of the steady flow at depth 0.07, plotted over the steady temperature field at the same depth. For (b), the sub-critical case S2 (contour interval 1.5×10^{-6}, 20 color contours from -0.07 to 0.07) and for (c) the supercritical case T1, after removal of the homogeneous steady flow and steady temperature field from case q00 (contour interval 0.0003, 20 color contours from -3.1 to -2.4).

displaced roughly 20° to the west when convection is present. Gibbons and Gubbins (2000) and Olson and Christensen (2002) have exhibited a dependence of this shift with the Ekman number. We argue here that the relevant parameter is the Peclet number of the flow (see (14)), because the shift crucially depends on temperature advection. To illustrate this, we use all cases with Y_2^2 heat flow pattern, including a sub-critical case. All control parameters are therefore varying. The westward shift is measured between the heat flux maxima/minima and the closest vortices, in both northern and southern hemispheres. This yields a set of eight results for each case, the mean and standard deviation of which are plotted versus *Pe* in Fig. 5. The sub-critical Y_2^2 case has almost no shift,

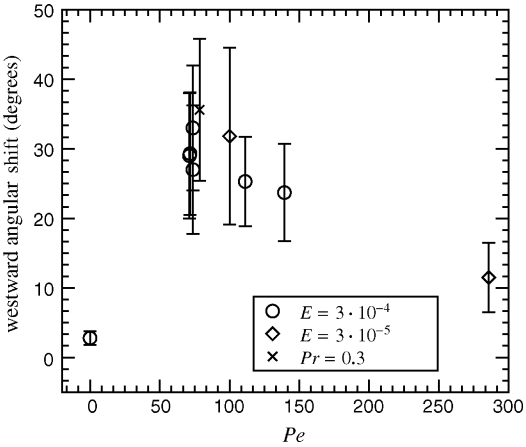

Fig. 5. Y_2^2 heat flow pattern. Westward longitudinal shift between the heat flow pattern and the streamfunction pattern, as a function of the Peclet number *Pe*. The error bars reflect the standard deviation of the angular shift in the set of 8 vortices (4 north, 4 south) created by a Y_2^2 heat flow pattern. The deviation is overestimated due to the asymmetric character of cyclones and anticyclones.

which strongly suggests that the shift is resulting from the advection of temperature patches by the underlying dynamo flow, away from the imposed heat flow location. As the Peclet number increases, the shift increases due to a coherent advection. The shift then reaches a maximum and decreases for large values of *Pe*, because advection becomes of smaller scale and less coherent. We, therefore, expect that the temperature patches reach zero shift with respect to the heat flux patches as mixing becomes complete in the large Peclet number limit which is relevant for the Earth's core.

3.2. The intermediate flows

Figs. 6 and 7 present streamfunctions representations of flows at the top of the free stream for cases q06 and q02, corresponding to high ($q^* = 0.625$) and low ($q^* = 0.2$) levels of mantle control, respectively, for a constant value of Ra_κ. In both cases a single harmonic Y_2^2 is used as boundary heterogeneity. Y_2^2 was chosen because it is the largest single harmonic in the mantle tomography model of Masters et al. (2000). In

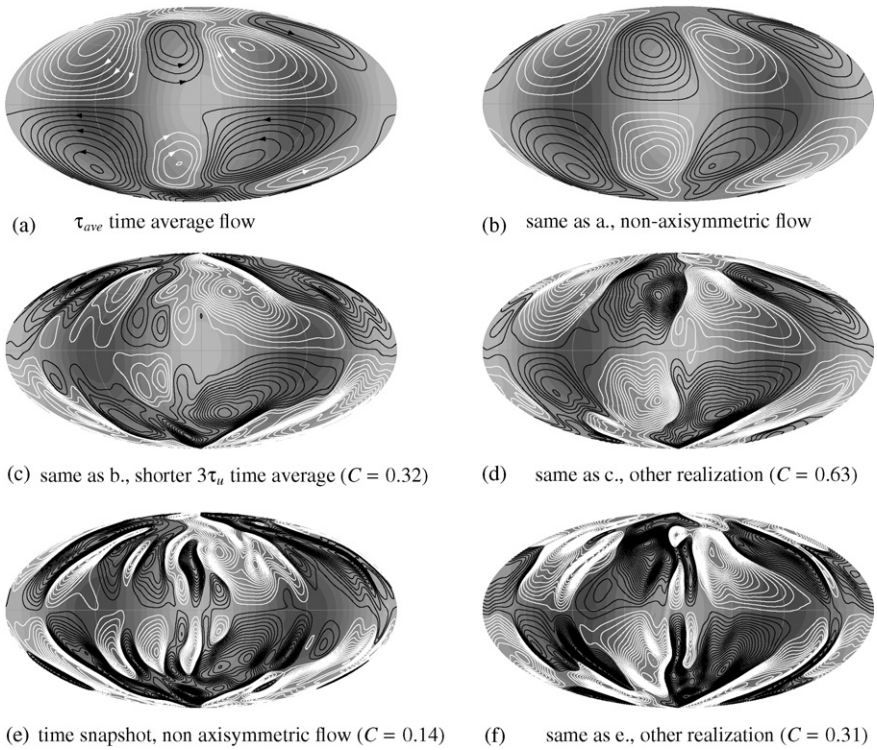

Fig. 6. Case q06 (high level of mantle control $q^* = 0.625$) streamfunction representations of flows at depth 0.07, plotted over heat flow pattern (larger than average outwards heat flow in light grey), (a) steady flow obtained by averaging over τ_{ave}. (b) Only the non-axisymmetric part of the flow, corresponding to the effect of the heterogeneous boundary condition, is selected as a reference for correlation. (c and d) Two realizations of intermediate averaging over a time $3\tau_u$ corresponding to three vortex turnover times (non-axisymmetric part of the flow). (e and f) Time snapshots from realizations (c and d), respectively. The vector correlation coefficient *C* with (b) is reported in (c, d, e and f). Contour interval in all plots is 0.0003.

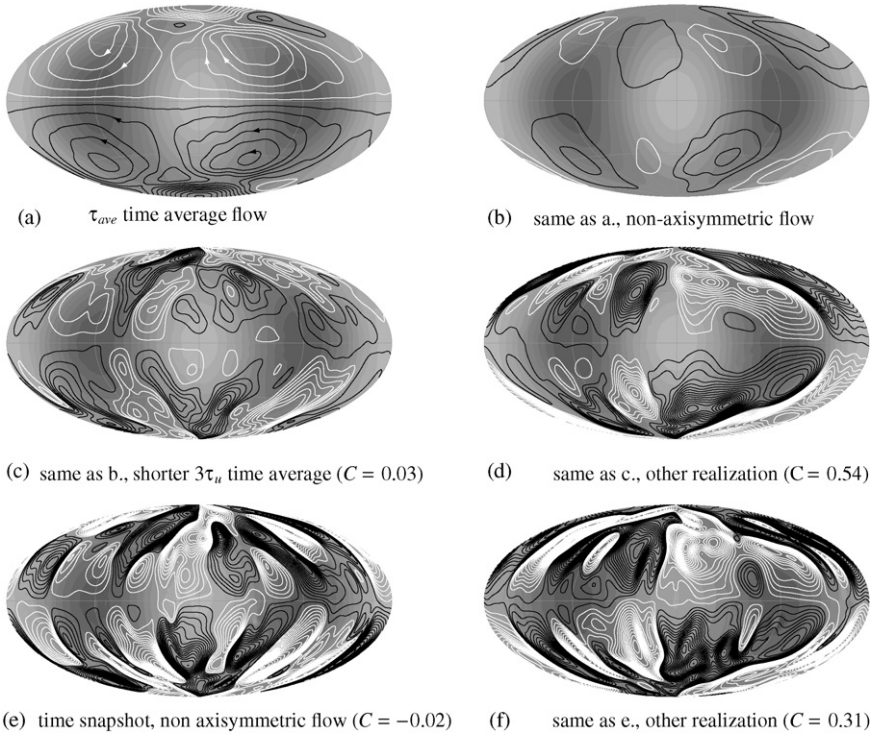

Fig. 7. Same as Fig. 6, for case q02 (low level of mantle control $q^* = 0.2$).

Figs. 6 and 7a, the steady flow pattern previously found by Olson and Christensen (2002) is recalled. In order to remove spurious correlations associated with the homogeneous dynamo, only the non-axisymmetric part of the flow (Figs. 6 and 7b) is taken as reference for subsequent analysis. A flow will be considered to carry a signature of mantle control if its non-axisymmetric part has a statistically significant correlation with this reference flow.

Figs. 6 and 7c and d show two intermediate flows obtained using time averaging over $3\tau_u$ units of time. These flows carry a significant transient part (see the higher density of streamlines compared to the reference flow (Figs. 6 and 7b) which is richer in smaller length scales. This transient flow is responsible for the time variability of the vector correlation coefficient C, which may vary from low (Figs. 6 and 7c) to high (Figs. 6 and 7d) values. In the case of high correlation, a qualitative visual check also indicates that the reference heterogeneity pattern and reference flow can indeed be seen in the intermediate flows. Comparing cases q06 and q02, we show that when the mantle control is large as in case q06, the correlation coefficient between the intermediate and reference flow is generally higher than when the mantle control is low as in case q02, which is an intuitive result. A somewhat more counter-intuitive and interesting result is revealed by case q02 in Fig. 7: the intermediate flow in Fig. 7d is much stronger in amplitude (by roughly a factor 10) than the steady flow in Fig. 7b, yet the two flows are highly correlated with $C = 0.54$. This shows that a weak level of mantle control can have a dramatic influence on the shape of the observable flow in this realization of intermediate time averaging. However, of course, an observer of the Earth core could be less fortunate and see a realization such as the one shown in Fig. 7c where the signature of mantle control has been lost ($C = 0.03$).

Figs. 6 and 7e and f present snapshots of flows captured within the intermediate time averaging of Figs. 6 and 7c and d, respectively. Snapshots are even richer in smaller length scales than intermediate averages. This underlines the importance of time-averaging, even over a short period of time such as $3\tau_u$: the resulting flows have higher correlation with the reference flow than snapshots, increasing significantly our chances to witness some mantle control.

3.3. Possibility of mantle control on intermediate flows

We anticipate that a key parameter to determine the correlation coefficient C is the relative amplitude A of the steady thermal wind with respect to the underlying

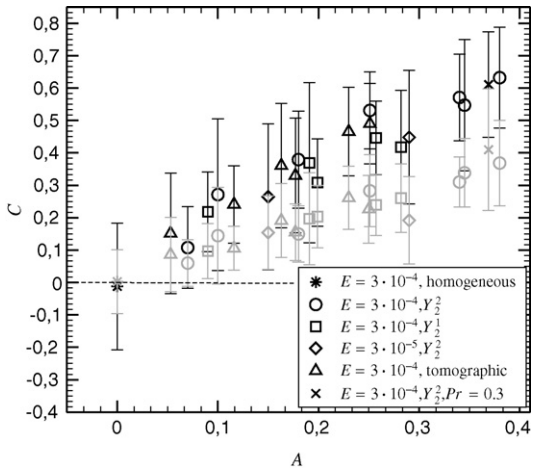

Fig. 8. Vector correlation coefficient C between steady thermal wind and transient flow at the outer surface of the model, as a function of the scaling parameter $A = U_{\text{ave}}/U$, describing the relative amplitude of the steady surface thermal wind and the underlying flow. Grey points are snapshots, black points are $3\tau_u$ intermediate time-averages. Points and error bars respectively represent the mean and standard deviation in a set of ten realizations.

dynamo flow, expressed as:

$$A = \frac{U_{\text{ave}}}{U} \tag{34}$$

where U_{ave} and U are respectively defined by (18) and (13). Fig. 8 shows a plot of C versus A, covering all cases in our data set. Points and error bars represent the mean and standard deviation of the correlation level in a set of ten realizations, for intermediate averages (black) and snapshots (grey). Generally we found positive correlation between intermediate and steady flows for all non-zero values of q^* which we investigated. The correlation C is increasing with A for a given heat flow pattern. Cases with different Ekman and Prandtl numbers, and with different heterogeneity patterns delineate the same trend curve, supporting the choice of A as a scaling parameter. Snapshots generally show about half the level of correlation seen for intermediate time averages.

4. Discussion

The novel approach of our study is to model time-average core flows from numerical dynamos with non-uniform boundary heat flow on two distinct time scales. On a long time scale representative of complete thermal mixing, a steady thermal wind arises, which is representative of the heterogeneous boundary heat flow pattern. The Lorentz, inertial and viscous forces have only a secondary influence. The thermal wind balance allowed us to propose and test a scaling law for this steady flow. In order to test the effect of an incomplete time-averaging, we have introduced the concept of intermediate flow, which we computed here for various simulations by taking averages over three vortex turnover times, presumably equivalent to 100–360 years in the Earth's core. Such intermediate flows are affected by both the steady flow and a transient flow from the underlying convective dynamo. We quantified the resemblance of steady and intermediate flow with a correlation coefficient, which we showed to be primarily dependent on the amplitude ratio of the two flows.

The generally positive character of the correlation between intermediate and steady flows suggests the possibility to observe thermal mantle control on the Earth's core on time scales related to flow advection. This is an encouraging perspective in light of the reliable SV inversion flow data, which have currently a timespan of roughly 150 years and could reach longer intervals when issues concerning geomagnetic data prior to 1840 are addressed, such as a re-evaluation of the magnetic field intensity (Gubbins et al., 2006). This is also consistent with the early suggestion of Bloxham and Gubbins (1987) that lateral temperature heterogeneities could be sufficient to force mantle-driven core convection. Here we may push the argument further by providing a quantification of this likeliness, and suggesting that the needed observation time is within the existing period of reliable historical geomagnetic data. To do this we estimate the relative amplitude $A = \tilde{U}_{\text{ave}}/\tilde{U}$ of the mantle-driven flow at the Earth's core surface and the underlying dynamo flow.

We may start by providing an estimate of the heat flow heterogeneity at the top of the Earth's core, from the mantle side of the CMB. Due to subducting plate material, lateral temperature heterogeneities there are thought to be quite considerable (Labrosse, 2002). Trampert et al. (2004) have attempted a separation of the thermal and chemical part of the seismic velocity heterogeneity. They found zero-to-peak lateral temperature variations of the order of 100 K. For the present estimation we will retain a peak-to-peak temperature variation of $\delta T = 200$ K. The thickness $\delta_m = 100$ km of the thermal boundary layer at the bottom of the mantle can be estimated using the thermal diffusion length $\delta_m = \sqrt{\kappa_m D_m/u_m}$, with the mantle velocity, thermal diffusivity and size being respectively taken as $u_m = 1$ cm/year, $D_m = 3000$ km and $K_m = 10^{-6}$ m^2/s (Schubert et al., 2001). Fourier's law then allows us to infer the heat flux heterogeneity across the core-mantle boundary:

$$\delta q = \rho_m C_{pm} \kappa_m \frac{\delta T}{\delta_m} \tag{35}$$

Using the mantle specific heat and density values $C_{pm} = 1000\,\mathrm{J\,K\,kg^{-1}}$ (Schubert et al., 2001) and $\rho_m = 5000\,\mathrm{kg/m^3}$ from PREM (Dziewonski and Anderson, 1981) we get $\delta q = 10\,\mathrm{mW/m^2}$. Compared to a reasonable value for the superadiabatic heat flow out of the Earth core of $q_0 = 15\,\mathrm{mW/m^2}$ (Labrosse, 2002), this represents a level of heterogeneity $q^* = \delta q/2q_0 = 30\%$.

On the core side the thickness $\tilde{\delta}$ of the thermal boundary layer is estimated using our best fit for (33). Using $D = 2200\,\mathrm{km}$, $\alpha = 10^{-5}\,1/\mathrm{K}$, $C_\mathrm{p} = 800\,\mathrm{J\,kg\,K^{-1}}$, and $\kappa = 5 \times 10^{-6}\,\mathrm{m^2/s}$ (Stacey, 1992), $\rho = 10^4\,\mathrm{kg/m^3}$ and $g_0 = 10\,\mathrm{m/s^2}$ (Dziewonski and Anderson, 1981), we get $Ra_\kappa = 7$, $E_\kappa = 10^{-14}$ and finally $\tilde{\delta} = 3$ m. Christensen and Aubert (2006) found a value of 10^6 for the Nusselt number Nu, which is equivalent to the ratio $D/\tilde{\delta}$. This is in agreement with our estimate for $\tilde{\delta}$. It differs strikingly from a thermal diffusion length estimate such as done previously for the mantle, which would yield $\tilde{\delta} \approx 100\,\mathrm{m}$, as previously used by Bloxham and Gubbins (1987). The point here is that rotating convection is quite different from Rayleigh-Bénard convection, and that Taylor columns have a tendency to break the conventional thermal boundary layer so as to shrink it towards the typical size of a viscous Ekman layer. This obviously appears only if the thickness of the thermal boundary layer is larger than that of the Ekman viscous boundary layer. The thickness of the Ekman layer is $DE^{1/2}$ (Greenspan, 1968). Using a core viscosity of $\nu = 10^{-6}\ \mathrm{m^2/s}$ (Stacey, 1992), we have $E = 2 \times 10^{-15}$, which gives an Ekman layer of thickness 10 cm. The thermal boundary layer is therefore expected to be still thicker than the Ekman layer, as already suggested by Christensen and Aubert (2006).

We next write the dimensional form of the thermal wind scaling (27) with its theoretical prefactor, and preserving its original form (23) as a force equilibrium:

$$2\Omega\tilde{U}_\mathrm{ave} = \alpha g_0 \frac{\delta q \tilde{\delta}}{\rho C_\mathrm{p} \kappa} \tag{36}$$

With the values previously used, we find $\tilde{U}_\mathrm{ave} = 5 \times 10^{-4}\mathrm{m/s}$. This is quite sizeable compared to our estimate $\tilde{U} = 6 \times 10^{-4}$ to $2 \times 10^{-3}\mathrm{m/s}$ for the root-mean-squared velocity inside the Earth's core. The amplitude ratio $A = \tilde{U}_\mathrm{ave}/\tilde{U} = 0.2 - 0.7$ is quite favourable, suggesting a level of correlation $C > 0.3$ between the intermediate and mantle-driven flow. Obviously we can only specify an order of magnitude for A, especially if we add uncertainties concerning the determination of U_ave which we have not included yet. Two factors might be underestimated and could yield an even stronger value for A. The peak-to-peak lateral temperature heterogeneity could be as large as 600 K (Trampert et al., 2004), and the penetration depth $\tilde{\delta}$ could also be larger, but not possibly much smaller than our estimate, since it already reaches down to the typical Ekman layer thickness. On the other hand, the prefactor for (27) lies between 0.33 and 0.72, depending on the boundary heat flow pattern, which could yield somewhat (but not by an order of magnitude) lower values for A. We conclude that the amplitude ratio lies in the range $0.1 < A < 1$, yielding a mean correlation level $C > 0.2$. This therefore suggests that the presence of a mantle signature in intermediate flows is quite likely.

A common drawback of scaling approaches is that we have to extrapolate a long way to reach Earth-like parameter values. This is not the case for scaling (27). For the Earth's core we have estimated $Ra_\kappa = 7$ and $q^* = 30\%$. The numerical models typically use the same q^*, and lower Ra_κ than in the Earth's core, but the key parameter to scale U_ave is the product $q^* Ra_\kappa \approx 2$, which is close to the range 0–0.5 explored by our models. There is more concern about scaling (33) for δ, in which the thermal Ekman number enters, with model values still remote from the Earth's core value $E_\kappa = 10^{-14}$. However, this scaling is derived from Christensen and Aubert (2006), who validated their approach over a broad parameter range. Finally, The Earth-like range of the output parameter A coincides with the explored range.

Our study suggests that core flows on centennial time scales are an important intermediate step between the geomagnetic data and their interpretation in terms of heterogeneous mantle control. We hope to motivate further work, both in the direction of core flow models and other coupling mechanisms between the core and the mantle.

Acknowledgements

Numerical calculations of this study were performed at the Service de Calcul Par-allele, IPGP, Paris, France. We are grateful to Peter Olson for stimulating discussions on this work. We also would like to thank two anonymous referees for comments which significantly improved the manuscript. This is IPGP contribution number 2180.

References

Amit, H., Olson, P., 2004. Helical core flow from geomagnetic secular variation. Phys. Earth Planet. Int. 147, 1–25.

Amit, H., Olson, P., 2006. Time average and time dependent parts of core flow. Phys. Earth Planet. Int. 155, 120–139, doi:10.1016/J.pepi.2005.10.006.

Aubert, J., 2005. Steady zonal flows in spherical shell dynamos. J. Fluid. Mech. 542, 53–67.

Bloxham, J., 2002. Time-independent and time-dependent behaviour of high-latitude flux bundles at the core-mantle boundary. Geophys. Res. Let 29 (18), 1854.

Bloxham, J., Gubbins, D., 1985. The secular variation of Earth's magnetic field. Nature 317, 777–781.

Bloxham, J., Gubbins, D., 1987. Thermal core-mantle interactions. Nature 325, 511–513.

Bloxham, J., Jackson, A., 1990. Lateral temperature variations at the core-mantle boundary deduced from the magnetic field. Geophys. Res. Let. 17, 1997–2000.

Bloxham, J., Jackson, A., 1991. Fluid flow near the surface of Earth's outer core. Rev. Geophys. 29, 97–120.

Bouligand, C., Hulot, G., Khokhlov, A., Glatzmaier, G.A., 2005. Statistical paleomagnetic field modeling and dynamo numerical simulation. Geophys. J. Int. 161, 603–626.

Carlut, J., Courtillot, V., 1998. How complex is the time-averaged geomagnetic field over the past 5 Myr? Geophys. J. Int. 134, 527–544.

Christensen, U., Aubert, J., 2006. Scaling properties of convection-driven dynamos in rotating spherical shells and application to planetary magnetic fields. Geophys. J. Int. 117, 97–114, doi:10.1111/j.l365-246X.2006.03009.x.

Christensen, U., Olson, P., 2003. Secular variation in numerical geodynamo models with lateral variations of boundary heat flux. Phys. Earth Planet. Int. 138, 39–54, doi:10.1016/S0031-9201(03)00064-5.

Christensen, U., Tilgner, A., 2004. Power requirement of the geodynamo from ohmic losses in numerical and laboratory dynamos. Nature 429, 169–171, doi:10.1038/nature02508.

Constable, C., Johnson, C., Lund, S., 2000. Global geomagnetic field models for the past 3000 years: transient or permanent flux lobes? Phil. Trans. Roy. Soc. A 358, 991–1008.

Dziewonski, A., Anderson, D., 1981. Preliminary reference Earth model PREM. Phys. Earth Planet. Int. 25, 297–356.

Eymin, C., Hulot, G., 2005. On core surface flows inferred from satellite magnetic data. Phys. Earth Planet. Int. 152, 200–220.

Gibbons, S., Gubbins, D., 2000. Convection in the Earth's core driven by lateral variation in the core-mantle boundary heat flux. Geophys. J. Int. 142, 631–642.

Greenspan, H.P., 1968. The Theory of Rotating Fluids. Breukelen Press.

Gubbins, D., Kelly, P., 1993. Persistent patterns in the geomagnetic field over the past 2.5 Myr. Nature 365, 829–832.

Gubbins, D., Jones, A.L., Finlay, C., 2006. Fall in Earth's magnetic field is erratic. Nature 312, 900–902.

Hide, R., 1970. On the Earth's core-mantle interface. Q. J. R. Meterol. Soc 96, 579–590.

Hongre, L., Hulot, G., Khokhlov, A., 1998. An analysis of the geomagnetic field over the past 2000 years. Phys. Earth Planet. Int. 106, 311–335.

Hulot, G., Bouligand, C., 2005. Statistical paleomagnetic field modeling and symmetry considerations. Geophys. J. Int. 161, 591–602.

Hulot, G., Le Mouël, J.-L., 1994. A statistical approach to the Earth's main magnetic field. Phys. Earth Planet. Int. 82, 167–183.

Hulot, G., Eymin, C., Langlais, B., Mandea, M., Olsen, N., 2002. Small-scale structure of the geodynamo inferred from Oersted and Magsat satellite data. Nature 416, 620–623.

Jackson, A., Jonkers, A.R.T., Walkers, M.R., 2000. Four centuries of geomagnetic secular variation from historical records. Phil. Trans. Roy. Soc. A 358, 957–990.

Johnson, C., Constable, C., 1995. The time averaged geomagnetic field as recorded by lava flows over the past 5 Myr. Geophys. J. Int. 112, 489–519.

Jones, G.M., 1977. Thermal interaction of the core and the mantle and long-term behaviour of the geomagnetic field. J. Geophys. Res. 82, 1703–1709.

Khokhlov, A., Hulot, G., Bouligand, C., 2006. Testing statistical paleomagnetic field models against directional data affected by measurement error. Geophys. J. Int. 167 (2), 635–648.

Korte, M., Genevey, A., Constable, C., Frank, U., Schnepp, E., 2005. Continuous geomagnetic field models for the past 7 millenia: 1. A new global data compilation. Geochem. Geophys. Geosyst. (G-cubed) 6, doi:10.1029/2004GC000800.

Labrosse, S., 2002. Hotspots, mantle plumes and core heat loss. Earth Planet. Sci. Lett. 199, 146–156.

Le Huy, M., Mandea, M., Le Mouël, J.-L., Pais, A., 2000. Time evolution of the fluid flow at the top of the core, geomagnetic jerks. Earth Planets Space 52, 163–173.

Le Mouël, J.-L., Jault, D., Gire, C., Madden, T., 1985. Motions of the core surface in the geostrophic approximation. Phys. Earth Planet. Int. 39, 270–287.

Masters, G., Laske, G., Bolton, H., Dziewonski, A., 2000. The relative behavior of shear velocity, bulk sound speed, and compressional velocity in the mantle: implications for chemical and thermal structure. In: Karato, S., Forte, A.M., Liebermann, R.C., Masters, G., Stixrude, L., (Eds.), Earth's Deep Interior, vol. 117, AGU Monograph, Washington D.C.

McElhinny, M., McFadden, P., Merrill, R., 1996. The time-averaged paleomagnetic field 0–5 mA. J. Geophys. Res. 101, 25007–25027.

Olson, P., Christensen, U., 2002. The time averaged magnetic field in numerical dynamos with non-uniform boundary heat flow. Geophys. J. Int. 151, 809–823.

Olson, P., Glatzmaier, G.A., 1996. Magnetoconvection and thermal coupling of the Earth's core and mantle. Phil. Trans. Roy. Soc. A 354, 1413–1424.

Pais, A., Hulot, G., 2000. Length of day decade variations, torsional oscillations and inner core superrotation: evidence from recovered core surface zonal flows. Phys. Earth Planet. Int. 118, 291–316.

Schubert, G., Turcotte, D., Olson, P., 2001. Mantle Convection in the Earth and planets. Cambridge University Press.

Stacey, F.D., 1992. Physics of the Earth. Brookfield Press.

Trampert, J., Deschamps, F., Resovsky, J., Yuen, D., 2004. Probabilistic tomography maps chemical heterogeneities throughout the lower mantle. Science 306, 853–856.

Wicht, J., 2002. Inner-core conductivity in numerical dynamo simulations. Phys. Earth Planet. Int. 132, 281–302.

Zhang, K., Gubbins, D., 1992. On convection in the Earth's core driven by lateral temperature variations in the lower mantle. Geophys. J. Int. 108, 247–255.

Zhang, K., Gubbins, D., 1993. Nonlinear aspects of core-mantle interaction. Geophys. Res. Let. 20, 2969–2972.